Check for updates

# Hierarchical wave-mode separation in the poroelastic medium using eigenform analysis

Yiwei Tian[1], Jidong Yang[1], Zhenchun Li[1], Jianping Huang[1], and Shanyuan Qin[1]

## ABSTRACT

In the elastic medium, the scalar and vector P- and S-waves decomposition has been extensively studied and some strategies can be extended to the poroelastic medium to extract P- and S-wavefields. However, there are three propagation modes in the poroelastic medium in Biot's theory, namely, a fast P wave, a slow P wave, and an S wave. Because the propagation characteristic of a slow P wave is different from that of a fast P wave and S wave, the wavefield separation methods in the elastic medium cannot be directly applied to the poroelastic medium to produce a complete wave-mode separation. Based on the eigenform analysis, we have developed a hierarchical wavefield decomposition method to completely separate S waves and fast and slow P waves in the poroelastic medium. Using the Helmholtz decomposition, we first compute scalar and vector potential wavefields to separate P and S waves. Then, a cross-product operator is proposed to decompose fast and slow P waves based on their different polarization directions. To produce correct amplitudes and phases, we apply another cross-product operator and an amplitude correction term to the separated wavefields. Three numerical examples demonstrate that our method can produce accurate fast P-wave, slow P-wave, and S-wave separation results, and the decomposed fast and slow P waves have the same phases and amplitudes as the P-wave potential wavefields.

## INTRODUCTION

In exploration seismology, subsurface rock is commonly considered as a single-phase acoustic or elastic medium (Aki and Richards, 2002). This hypothesis makes it relatively easy for seismic modeling, imaging, and inversion. However, the real subsurface medium, especially for sedimentary reservoirs, has a large number of pores filled with fluids (Biot, 1956a). The interactions between pore fluids and rock matrix have an important influence on seismic wave propagation (Biot, 1962; Johnson et al., 1987). Thus, taking account of the pore fluid effects helps to produce more accurate seismic modeling and imaging results for oil and gas reservoirs.

The poroelastic theory is a typical method to consider the effect of pore fluid and solid matrix in seismic wave propagation (Yang and Malcolm, 2021). In terms of spatial scale, the poroelastic theory can be categorized into macroscopic, mesoscopic, and microscopic scales (Carcione and Picotti, 2006). The basic wave equations have been proposed by Biot (1956a, 1956b), which provide an important foundation for describing elastic wave propagation in fluid-saturated porous media at the macroscopic scale. On this basis, some more robust equations (de la Cruz and Spanos, 1985; Sahay et al., 2001) have been presented to describe seismic wave phenomena at this scale. To explain the energy attenuation and phase dispersion during wave propagation, many modified models, including the squirt-flow model (Mavko and Nur, 1975, 1979), have been proposed at a microscopic scale. At the mesoscopic scale, the patchy saturation model is built to explain seismic attenuation in the low-frequency band (White, 1975; White et al., 1975; Carcione et al., 2003; Pride et al., 2004).

In the poroelastic medium, there are S waves and fast and slow P waves. One way to better understand the propagations of different wave modes and reduce crosstalk artifacts in imaging and inversion is based on wavefield decomposition. The decomposition of P and S waves has been extensively studied in the single-phase elastic medium. For instance, the Helmholtz decomposition is commonly used to extract the dilatational and rotational waves in early studies (Morse and Feshbach, 1954; Dellinger and Etgen, 1990). However, the divergence and curl operations change the phases and amplitudes of the separated wavefields compared with the coupled elastic wavefields. To mitigate this drawback, the vector wavefield decomposition is proposed by Zhang and McMechan (2010). Subsequently, different strategies have been developed to implement true-amplitude vector

wavefield decomposition. For instance, Xiao and Leaney (2010) introduce an auxiliary P-wave equation and calculate the S-wavefield by subtracting the P-wavefield from elastic wavefields (Wang and McMechan, 2015; Du et al., 2017). Zhu (2017) corrects the phases and amplitudes by solving Poisson's equation, and Yang et al. (2018) improve this method by introducing an amplitude and phase correction strategy. Currently, the vector wavefield decomposition method has been extended to the anisotropic medium (Cheng and Fomel, 2014; Sripanich et al., 2017; Wang et al., 2018; Yang et al., 2019).

Some separation strategies in the elastic medium also can be extended to the poroelastic medium. For example, Biot (1956a) obtains P- and S-wavefields using the Helmholtz decomposition. Chen (2011) applies a first-order velocity-stress elastic wavefield separation scheme to Biot's equations to separate pure P- and S-wavefields. However, because the coupling of different wave modes is more complex in the poroelastic medium than in the elastic medium, few previous studies have been done to separate the three wave modes. To support imaging and inversion in the poroelastic medium, it is necessary to develop a complete separation method for S waves and fast and slow P waves.

In this study, we apply the eigenform analysis to the poroelastic wave equations and propose a hierarchical wave-mode separation method. The Helmholtz decomposition is first applied to compute the P- and S-wave potential fields. Then, the eigenvalues and eigenvectors of the P-wave potentials for the fluid and solid phases are calculated to extract the fast and slow P waves. Because the polarization directions of fast and slow P waves are not orthogonal, a cross-product operator associated with the eigenvectors is proposed to separate fast and slow P-wave modes, followed by applying another cross product and an amplitude correction to produce true-amplitude potential wavefields of the fluid and solid phases. Numerical examples for a homogeneous model, a simple layered model, and the complicated Marmousi model demonstrate that the proposed method can accurately separate S-wavefields and fast and slow P-wavefields for poroelastic media.

The rest of this paper is organized as follows. First, we give a brief review of the poroelastic wave equation. Then, we present the details of the proposed hierarchical wavefield separation method. Finally, numerical examples are used to illustrate the performance of our method.

## METHODOLOGY

### Review of Biot's poroelastic wave equations

To describe seismic wave propagation in a porous elastic solid filled with saturated fluid, Biot (1956a) proposes the following wave equations:

$$N\nabla^2\mathbf{u}_s + \text{grad}\left[(A+N)\left(\frac{\partial u_x^s}{\partial x} + \frac{\partial u_z^s}{\partial z}\right) + Q\left(\frac{\partial u_x^f}{\partial x} + \frac{\partial u_z^f}{\partial z}\right)\right]$$
$$= \frac{\partial^2}{\partial t^2}(\rho_{11}\mathbf{u}_s + \rho_{12}\mathbf{u_f}) + B\frac{\partial}{\partial t}(\mathbf{u}_s - \mathbf{u_f}),$$
$$\text{grad}\left[Q\left(\frac{\partial u_x^s}{\partial x} + \frac{\partial u_z^s}{\partial z}\right) + R\left(\frac{\partial u_x^f}{\partial x} + \frac{\partial u_z^f}{\partial z}\right)\right]$$
$$= \frac{\partial^2}{\partial t^2}(\rho_{12}\mathbf{u}_s + \rho_{22}\mathbf{u_f}) - B\frac{\partial}{\partial t}(\mathbf{u}_s - \mathbf{u_f}), \quad (1)$$

where $\mathbf{u}_s = [u_x^s, u_z^s]^T$; $\mathbf{u}_f = [u_x^f, u_z^f]^T$; $u_x^s$ and $u_z^s$ are the x- and z-component displacement of the solid phase, respectively; and $u_x^f$ and $u_z^f$ are for the fluid phase. The A, N, Q, and R are the elastic coefficients, $\rho_{11}$, $\rho_{12}$, and $\rho_{22}$ are mass coefficients, and B is the coefficient of dissipation. The detailed expressions of these parameters can be found in Biot (1956a). This equation accounts for the properties of solid skeleton and pore fluid and can be used to accurately describe the propagation of seismic waves in a two-phase medium. Based on equation 1, two types of dilatational waves have been observed, which are known as fast and slow P waves. The energy of the slow P waves in the fluid phase is stronger than that in the solid phase, and the propagation speed is determined by porosity (Zhu and McMechan, 1991). Therefore, there exist three types of waves in Biot's theory, i.e., S wave and fast and slow P wave, and they are coupled together. Using the eigenform analysis (Yang et al., 2019), we present a complete wave-mode decomposition method for the poroelastic medium in the following section.

### Eigenform analysis for Biot's wave equation

Without considering the dissipation, Biot's equation 1 can be rewritten as

$$N\nabla^2\mathbf{u}_s + \text{grad}\left[(A+N)\left(\frac{\partial u_x^s}{\partial x} + \frac{\partial u_z^s}{\partial z}\right) + Q\left(\frac{\partial u_x^f}{\partial x} + \frac{\partial u_z^f}{\partial z}\right)\right]$$
$$= \frac{\partial^2}{\partial t^2}(\rho_{11}\mathbf{u}_s + \rho_{12}\mathbf{u_f}),$$
$$\text{grad}\left[Q\left(\frac{\partial u_x^s}{\partial x} + \frac{\partial u_z^s}{\partial z}\right) + R\left(\frac{\partial u_x^f}{\partial x} + \frac{\partial u_z^f}{\partial z}\right)\right]$$
$$= \frac{\partial^2}{\partial t^2}(\rho_{12}\mathbf{u}_s + \rho_{22}\mathbf{u_f}). \quad (2)$$

Applying the divergence to equation 2, we can obtain the wave equations for the solid and fluid P-wave potentials as

$$\nabla^2[(A+2N)\theta_s + Q\theta_f] = \frac{\partial^2}{\partial t^2}(\rho_{11}\theta_s + \rho_{12}\theta_f),$$
$$\nabla^2[Q\theta_s + R\theta_f] = \frac{\partial^2}{\partial t^2}(\rho_{12}\theta_s + \rho_{22}\theta_f), \quad (3)$$

where $\theta_s = \nabla \cdot \mathbf{u}_s$ and $\theta_f = \nabla \cdot \mathbf{u}_f$ are the scalar potential wavefields. Equation 2 contains S waves and two kinds of P waves. The divergence removes the S-wavefields, and thus the resulting equation 3 only contains the fast and slow P waves. The S-wave mode can be extracted by applying a curl operation to equation 2. Here, we focus on the eigenform analysis for the slow and fast P waves.

By applying algebraic operations, equation 3 can be reformulated into an expression that is similar to the Christoffel equation in an elastic medium (the detailed derivation is given in Appendix A):

$$\nabla^2\{[(A+2N)\rho_{22}-Q\rho_{12}]\theta_s+[Q\rho_{22}-R\rho_{12}]\theta_f\}$$
$$=\frac{\partial^2}{\partial t^2}(\rho_{11}\rho_{22}-\rho_{12}^2)\theta_s,$$
$$\nabla^2\{[-(A+2N)\rho_{12}+Q\rho_{11}]\theta_s+[-Q\rho_{12}+R\rho_{11}]\theta_f\}$$
$$=\frac{\partial^2}{\partial t^2}(\rho_{11}\rho_{22}-\rho_{12}^2)\theta_f. \tag{4}$$

Transforming equation 4 into the frequency and wavenumber domain, we have

$$\begin{bmatrix} [(A+2N)\rho_{22}-Q\rho_{12}](k_x^2+k_z^2) & (Q\rho_{22}-R\rho_{12})(k_x^2+k_z^2) \\ [-(A+2N)\rho_{12}+Q\rho_{11}](k_x^2+k_z^2) & (-Q\rho_{12}+R\rho_{11})(k_x^2+k_z^2) \end{bmatrix}$$
$$\begin{bmatrix} \hat{\theta}_s \\ \hat{\theta}_f \end{bmatrix} = \frac{\rho_{11}\rho_{22}-\rho_{12}^2}{\omega^2}\begin{bmatrix} \hat{\theta}_s \\ \hat{\theta}_f \end{bmatrix}, \tag{5}$$

where $\hat{\theta}_s$ and $\hat{\theta}_f$ are the Fourier transform of $\theta_s$ and $\theta_f$, respectively; $k_x$ and $k_z$ are the horizontal and vertical wavenumbers, respectively; and $\omega$ is the angular frequency. For simplification, we define the coefficients on the left side of equation 5 as

$$\mathbf{M}=\begin{bmatrix} [(A+2N)\rho_{22}-Q\rho_{12}](k_x^2+k_z^2) & (Q\rho_{22}-R\rho_{12})(k_x^2+k_z^2) \\ [-(A+2N)\rho_{12}+Q\rho_{11}](k_x^2+k_z^2) & (-Q\rho_{12}+R\rho_{11})(k_x^2+k_z^2) \end{bmatrix}. \tag{6}$$

The eigenvalues of the matrix $\mathbf{M}$ have the form as

$$\lambda_{1,2}=\left(\frac{(A+2N)\rho_{22}-2Q\rho_{12}+R\rho_{11}}{2}\pm\frac{\sqrt{C+D}}{2}\right)(k_x^2+k_z^2), \tag{7}$$

with

$$C=(A+2N)^2\rho_{22}^2+2(A+2N)(2R\rho_{12}^2-R\rho_{11}\rho_{22}-2Q\rho_{12}\rho_{22}),$$
$$D=4Q\rho_{11}(Q\rho_{22}-R\rho_{12})+R^2\rho_{11}^2, \tag{8}$$

and the corresponding eigenvectors are

$$\hat{\mathbf{a}}_{\text{fast}}=\begin{bmatrix} \frac{1}{2}[(A+2N)\rho_{22}-R\rho_{11}+\sqrt{C+D}](k_x^2+k_z^2) \\ [-(A+2N)\rho_{12}+Q\rho_{11}](k_x^2+k_z^2) \end{bmatrix},$$
$$\hat{\mathbf{a}}_{\text{slow}}=\begin{bmatrix} (Q\rho_{22}-R\rho_{12})(k_x^2+k_z^2) \\ \frac{1}{2}[-(A+2N)\rho_{22}+R\rho_{11}-\sqrt{C+D}](k_x^2+k_z^2) \end{bmatrix}. \tag{9}$$

The detailed derivation is given in Appendix B. Each pair of the eigenvalue and eigenvector corresponds to one of the two wave modes, i.e., slow and fast P waves. The eigenvector represents the wavefield polarization direction.

Compared with the elastic case, the eigenform analysis for the poroelastic wave equation has the following differences. First, equation 9 shows that each component of the eigenvectors has a $k_x^2+k_z^2$ term. That means the propagation direction $(k_x,k_z)$ does not influ-

ence the polarization directions, and the eigenvectors are only determined by the model parameters. In contrast, the eigenvectors of the isotropic and anisotropic elastic medium are determined by model parameters and wave propagation direction $(k_x,k_z)$. Because the representation of eigenvectors is not unique, the eigenvectors of $\mathbf{M}$ can be simplified to

$$\hat{\mathbf{a}}_{\text{fast}}=\begin{bmatrix} \frac{1}{2}[(A+2N)\rho_{22}-R\rho_{11}+\sqrt{C+D}] \\ [-(A+2N)\rho_{12}+Q\rho_{11}] \end{bmatrix},$$
$$\hat{\mathbf{a}}_{\text{slow}}=\begin{bmatrix} Q\rho_{22}-R\rho_{12} \\ \frac{1}{2}[-(A+2N)\rho_{22}+R\rho_{11}-\sqrt{C+D}] \end{bmatrix}. \tag{10}$$

The removal of $k_x$ and $k_z$ in equation 10 makes it easier to numerically implement the slow and fast P-waves separation because the vectors can be used as the polarization operators directly. Because of the missing $k_x$ and $k_z$, here, we call the vectors in equation 10 quasi-polarization vectors. Second, the polarization directions of P and S waves are orthogonal in the isotropic and anisotropic elastic medium. However, equation 10 shows that the polarization directions of slow and fast P waves are not perpendicular to each other. This observation indicates that the scalar and vector of P- and S-wave separation methods developed in the elastic medium cannot be directly applied to the poroelastic medium to separate the slow and fast P waves.

## Slow and fast P-waves decomposition

In an elastic medium, P- or S-wave mode can be extracted by projecting the coupled elastic wavefields to their polarization directions. Mathematically, this can be implemented by applying a dot product for the wavefields and polarization vectors. For the slow and fast P waves, the polarizations are not orthogonal to each other. Projecting the solid and fluid potential wavefields to the polarization of one wave mode cannot eliminate the other wave mode. Therefore, the dot-product-based wavefield separation method is no longer suitable for separating slow and fast P waves.

The cross-product method also can be used for elastic wavefield separation. Applying a cross product of the polarization vector of one basic wave mode to the coupled wavefields will remove this type of wave and leave other types of wave. Thus, whether the polarization vectors of slow and fast P waves are orthogonal or not, we can use the cross-product operation to implement the wave-mode separation as

$$\mathbf{u}_{\text{slow}}=\mathbf{a}_{\text{fast}}\times\theta, \quad \mathbf{u}_{\text{fast}}=\mathbf{a}_{\text{slow}}\times\theta, \tag{11}$$

where $\mathbf{u}_{\text{slow}}$ and $\mathbf{u}_{\text{fast}}$ are the separated slow and fast wavefields, respectively; $\mathbf{a}_{\text{fast}}$ and $\mathbf{a}_{\text{slow}}$ are the fast and slow P-wave quasi-polarization vectors, respectively; $\theta=[\theta_s,\theta_f]^T$; and $\theta_s$ and $\theta_f$ are the solid and fluid P-wave potentials, respectively.

Although equation 11 can produce pure slow and fast P waves, a cross-product operation changes the phase and amplitude of the potential wavefields. To produce the phases and amplitudes, we apply another cross product and an amplitude correction term to the separated wavefields. This can be expressed as

$$\theta_{\text{slow}} = \frac{1}{|\mathbf{A}_{\text{slow}}|}(\mathbf{b}_{\text{slow}} \times \mathbf{u}_{\text{slow}}), \quad \theta_{\text{fast}} = \frac{1}{|\mathbf{A}_{\text{fast}}|}(\mathbf{b}_{\text{fast}} \times \mathbf{u}_{\text{fast}}),$$

(12)

where $\theta_{\text{slow}} = [\theta_{\text{slow}}^{\text{solid}}, \theta_{\text{slow}}^{\text{fluid}}]^T$ and $\theta_{\text{fast}} = [\theta_{\text{fast}}^{\text{solid}}, \theta_{\text{fast}}^{\text{fluid}}]^T$ are the slow and fast P waves, respectively, which have the same amplitudes and phases as $\theta$. The first components of $\theta_{\text{slow}}$ and $\theta_{\text{fast}}$ are the decomposed wavefields for the solid phase and the second components for the fluid phase. The $\mathbf{b}_{\text{slow}}$ is perpendicular to $\mathbf{a}_{\text{slow}}$ and $\mathbf{u}_{\text{slow}}$; $\mathbf{b}_{\text{fast}}$ is perpendicular to $\mathbf{a}_{\text{fast}}$ and $\mathbf{u}_{\text{fast}}$; $1/|\mathbf{A}_{\text{slow}}|$ and $1/|\mathbf{A}_{\text{fast}}|$ are the amplitude correction terms; and $|\mathbf{A}_{\text{slow}}|$ and $|\mathbf{A}_{\text{fast}}|$ are the determinants of the matrices $\mathbf{A}_{\text{slow}}$ and $\mathbf{A}_{\text{fast}}$, respectively, where $\mathbf{A}_{\text{slow}}$ and $\mathbf{A}_{\text{fast}}$ are the matrices constructed using the eigenvectors $\mathbf{a}_{\text{fast}}$ and $\mathbf{a}_{\text{slow}}$, respectively:

$$\mathbf{A}_{\text{slow}} = [\mathbf{a}_{\text{fast}} \quad \mathbf{a}_{\text{slow}}], \quad \mathbf{A}_{\text{fast}} = [\mathbf{a}_{\text{slow}} \quad \mathbf{a}_{\text{fast}}].$$

(13)

The method for determining $\mathbf{b}_{\text{slow}}$ and $\mathbf{b}_{\text{fast}}$ is given in Appendix C. The detailed derivation of $\mathbf{A}_{\text{fast}}$ and $\mathbf{A}_{\text{slow}}$ is given in Appendix D.

## Hierarchical wave-mode decomposition workflow in a poroelastic medium

For the poroelastic wavefields computed by solving Biot's equation 1, we first use the Helmholtz decomposition to extract P- and S-waves potential wavefields and then apply the cross-product-based separation method to produce pure slow and fast P waves. The hierarchical wave-mode separation is shown in Figures 1 and 2 and the workflow can be summarized as follows:

1) Applying the divergence and curl operations to poroelastic wavefields of solid and fluid phases to compute P- and S-waves potential fields as

$$\theta_s = \nabla \cdot \mathbf{u}_s, \quad \psi_s = \nabla \times \mathbf{u}_s,$$
$$\theta_f = \nabla \cdot \mathbf{u}_f, \quad \psi_f = \nabla \times \mathbf{u}_f,$$

(14)

where $\theta$ and $\psi$ are the P- and S-waves potentials, respectively, and subscripts $s$ and $f$ denote the solid and fluid phases, respectively.

2) Using the model parameters $A$, $N$, $Q$, and $R$ and the mass coefficients $\rho_{11}$, $\rho_{12}$, and $\rho_{22}$ to compute the eigenvectors according to equation 10.

3) Using the eigenvectors to construct vectors $\mathbf{a}_{\text{fast}}$ and $\mathbf{a}_{\text{slow}}$ as well as matrices $\mathbf{A}_{\text{fast}}$ and $\mathbf{A}_{\text{slow}}$ according to equation 13 and compute vectors $\mathbf{b}_{\text{fast}}$ and $\mathbf{b}_{\text{slow}}$ according to Appendix C.

4) Applying the double cross product with the amplitude correction term to the P-wave potentials to produce decomposed slow and fast P-wavefields according to equation 12.

## NUMERICAL EXAMPLES

In this section, we use three numerical examples to illustrate the feasibility and adaptability of the proposed wavefields separation method for a poroelastic medium.

### A homogeneous model

The elastic parameters of the homogeneous model are $V_{\text{P}}^{\text{solid}} = 3000$ m/s, $V_{\text{S}}^{\text{solid}} = 1732$ m/s, $\rho_{\text{solid}} = 2588$ kg/m³, $V_{\text{P}}^{\text{fluid}} = 1500$ m/s, $\rho_{\text{fluid}} = 952$ kg/m³, and $\phi = 0.15$, where $\phi$ is the porosity. The conversion formula from model parameters to Biot's parameters is given in Appendix E. The grid size of this model is $501 \times 501$ with a spatial interval of 10 m. The poroelastic wavefields are computed by solving Biot's two-phase wave equations using a staggered-grid finite-difference scheme (Virieux, 1984, 1986; Anthony and Vedanti, 2022). The source-time function is a Ricker wavelet with a dominant frequency of 10 Hz. A single force is applied to the vertical displacement at $x = 2.5$ km and $z = 2.5$ km, and a convolutional perfectly matched layer condition (Komatitsch and Martin, 2007) is used to absorb the boundary reflections.

In the poroelastic wavefields, the three wave modes, i.e., S wave and fast and slow P waves, can be clearly identified in Figure 3. The slow P waves have greater amplitudes in the fluid phase (Figure 3c
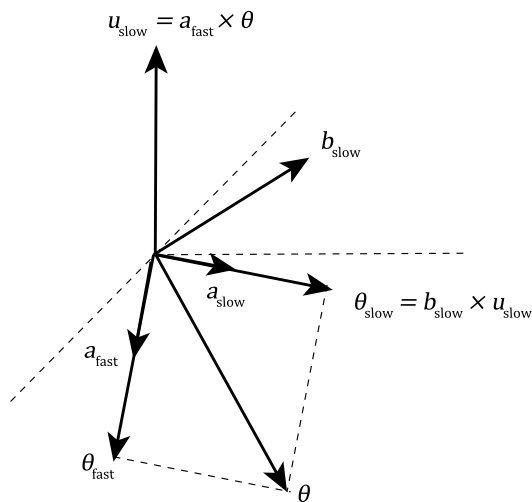


Figure 1. The procedure of decomposing the slow P waves in poroelastic theory. The polarization directions of fast and slow P waves are not perpendicular to each other. First, we use $\mathbf{a}_{\text{fast}} \times \theta$ to obtain the slow P-wavefield $\mathbf{u}_{\text{slow}}$. Then, we recover the amplitudes and phases by $(1/|\mathbf{A}_{\text{slow}}|)(\mathbf{b}_{\text{slow}} \times \mathbf{u}_{\text{slow}})$.
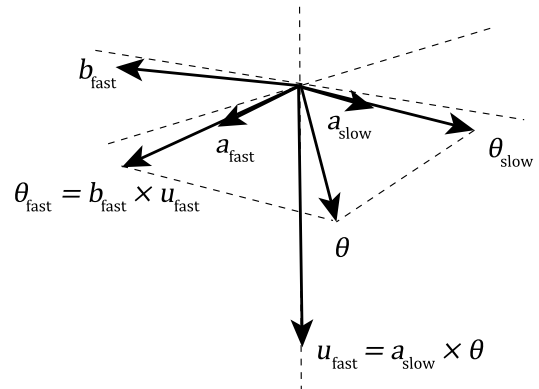


Figure 2. The procedure of decomposing the fast P waves in poroelastic theory. First, we use $\mathbf{a}_{\text{slow}} \times \theta$ to obtain the fast P-wavefield $\mathbf{u}_{\text{fast}}$. Then, we recover the amplitudes and phases by $(1/|\mathbf{A}_{\text{fast}}|)(\mathbf{b}_{\text{fast}} \times \mathbf{u}_{\text{fast}})$.

and 3d) than in the solid phase (Figure 3a and 3b), whereas the amplitudes of the fast P wave and S wave are similar in the two phases. Using the Helmholtz decomposition, we can extract the P and S waves, but the slow and fast P waves are still coupled in the P-wavefields of solid and fluid phases (Figure 4a and 4b). We then apply the proposed cross-product-based separation method
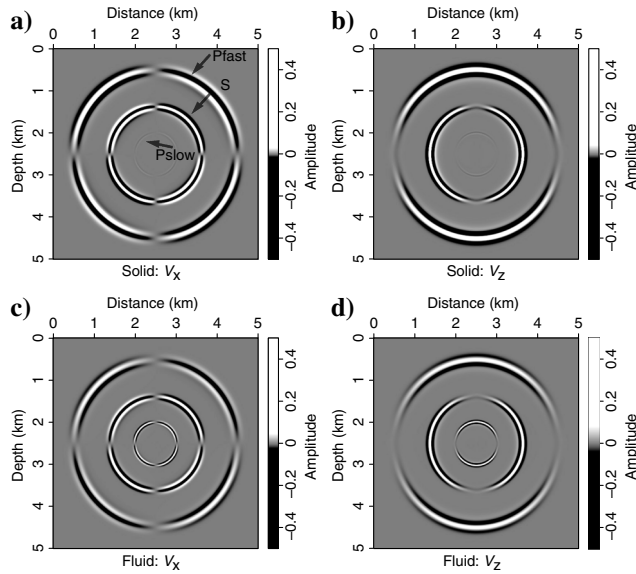
to P-wave potential fields. The results and residual wavefields are shown in Figure 5. The slow and fast P waves are decoupled completely. The amplitudes and phases of them are the same as those of the potential wavefields in Figure 4a and 4b. The residual wavefields in Figure 5e and 5f are computed by subtracting the separated slow and fast P waves from the coupled P-wave potential, which have a relative error of approximately $10^{-7}$. The proposed separation method has high accuracy in the homogeneous model.

## A two-layer model

The second example is a two-layer model. The upper parameters of the model are $V_P^{\text{solid}} = 2000$ m/s, $V_S^{\text{solid}} = 1150$ m/s, $\rho_{\text{solid}} = 2060$ kg/m$^3$, $V_P^{\text{fluid}} = 1500$ m/s, $\rho_{\text{fluid}} = 952$kg/m$^3$, and $\phi = 0.15$. The lower parameters of the model are $V_P^{\text{solid}} = 3000$ m/s, $V_S^{\text{solid}} = 1730$ m/s, $\rho_{\text{solid}} = 2280$ kg/m$^3$, $V_P^{\text{fluid}} = 1500$ m/s, $\rho_{\text{fluid}} = 952$ kg/m$^3$, and $\phi = 0.15$. The grid size of this model is $501 \times 501$ with a spatial interval of 10 m. The source-time function is a Ricker wavelet with a dominant frequency of 10 Hz. A vertical force at $x = 2.5$ km and $z = 2.5$ km is used to generate the vertical and horizontal component wavefields.

Figure 6 shows the components of velocity wavefields in the solid and fluid phases. When the wave propagates to the interface



Figure 3. Components of velocity wavefields in the homogeneous model. (a and b) Horizontal and vertical components of the solid phase, respectively. (c and d) Horizontal and vertical components of the fluid phase, respectively. There are three types of waves, fast P wave, S wave, and slow P wave, from the outer circle to the inner circle. The energy of the slow P wave in the fluid phase is stronger than in the solid phase.



Figure 4. Decomposed P-wavefields and S-wavefields based on Helmholtz decomposition. (a and b) P-wave potential wavefields obtained by the divergence operation in the solid and fluid phases, respectively. The fast and slow P waves are coupled in the P-wave potentials. (c and d) S-wavefields obtained by the curl operation in the solid and fluid phases, respectively.
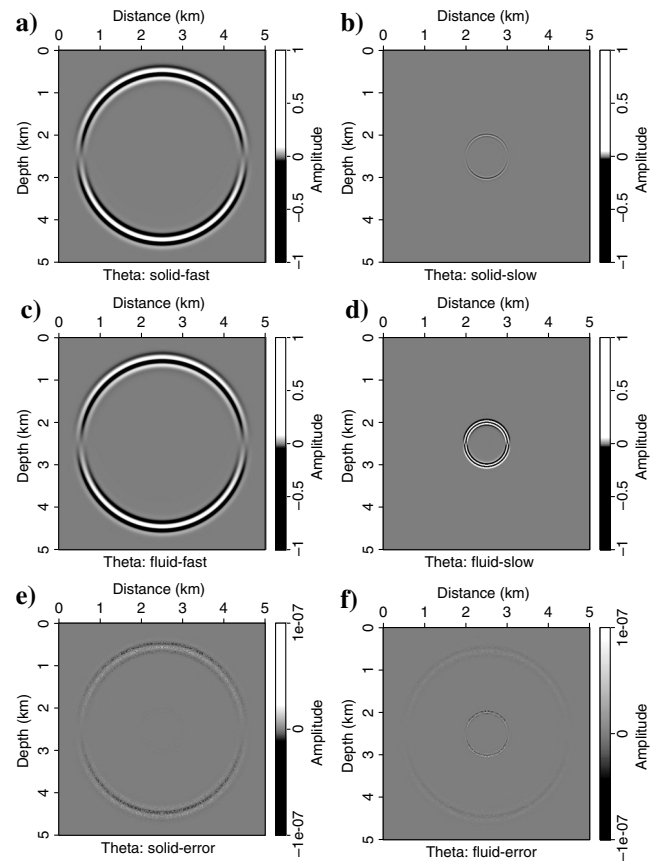


Figure 5. Decomposed fast and slow P-waves components in the homogeneous model. (a and b) The fast and slow P waves, respectively, the solid phase. (c and d) The fast and slow P waves, respectively, the fluid phase. The decomposition retains the amplitudes and phases. The errors (e and f) are mainly numerical artifacts and can be negligible.

in a poroelastic medium, reflection, transmission, and P-S conversion are generated. These waves are marked in Figures 7 and 8, where $T$ denotes transmission and $R$ denotes reflection. The separated P and S waves based on the divergence and curl operators are shown in Figure 7, where the S waves are converted from the fast and slow P waves and show the same radiation pattern in the two
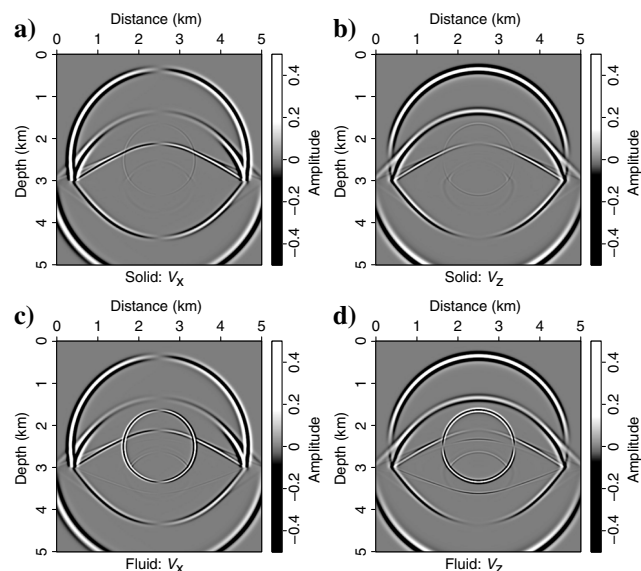
phases. We apply the proposed separation method to the P-wave potential wavefields; the results are shown in Figure 8. Note that, because of wave-mode conversion, the separated fast P-wavefields contain the direct fast P waves and the converted fast P waves, they are all separated from the slow P waves. It is the same for slow P waves. The decomposed fast and slow P-wavefields do not have crosstalk, and their amplitudes and phases are the same as the coupled P-wave potential wavefields. The differences between original coupled and separated wavefields (Figure 8e and 8f) are mainly numerical errors and can be negligible.

## Marmousi2 model

A portion of Marmousi2 is used to test the performance of the proposed method. The model parameters are shown in Figure 9. We set the center part of the model as the reservoir (the brown part in Figure 9f) filled with oil, and the other area is filled with water. A vertical force is applied at $x = 3.75$ km and $z = 1.5$ km.

Figure 10 shows the snapshots of the particle velocity wavefields. In this model, because of the large contrast in the velocity between



Figure 6. Components of velocity wavefields in the two-layer model. (a and b) Horizontal and vertical components of the solid phase, respectively. (c and d) Horizontal and vertical components of the fluid phase, respectively.
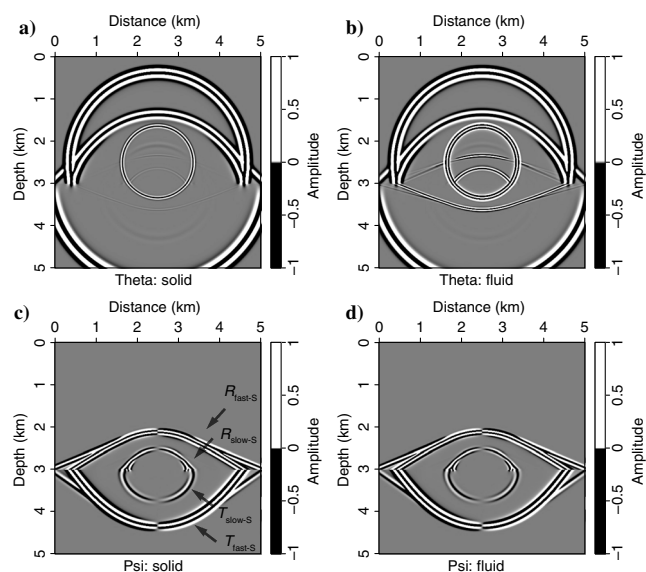


Figure 7. Decomposed P- and S-wave potentials based on Helmholtz decomposition in the two-layer model. (a and b) The solid and fluid phases of P-wave potentials, respectively. The fast and slow P waves are still coupled. (c and d) The S waves converted from the fast and slow P waves. The $R_{\text{fast-S}}$ is the reflected S wave converted from a fast P wave; $R_{\text{slow-S}}$ is the reflected S wave converted from a slow P wave; $T_{\text{fast-S}}$ is the transmitted S wave converted from the fast P wave; and $T_{\text{slow-S}}$ is the transmitted S wave converted from the slow P wave.
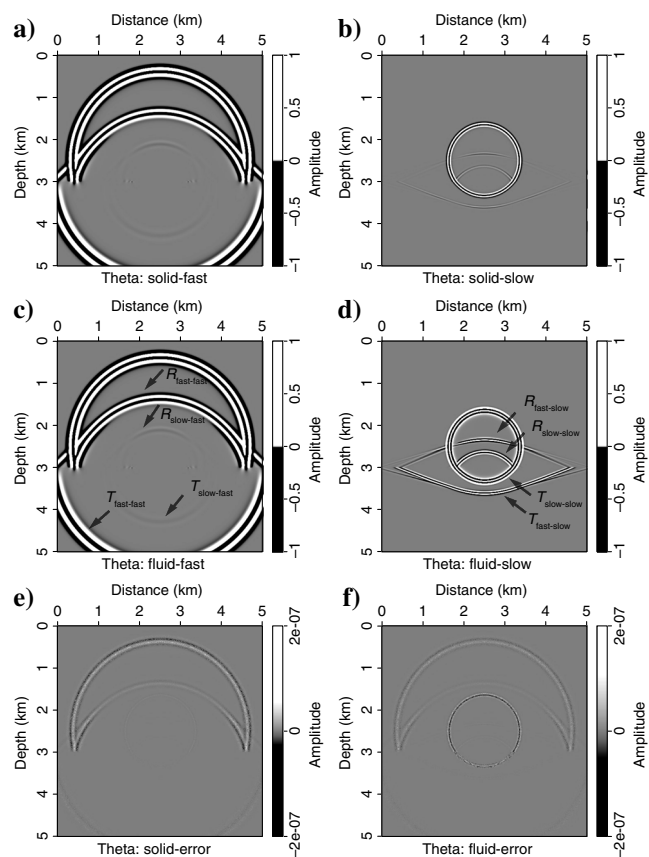


Figure 8. Decomposed fast and slow P-waves components in the two-layer model. (a and b) The fast and slow P waves in the solid phase, respectively. (c and d) The fast and slow P waves in the fluid phase, respectively. The $T$ denotes transmission and $R$ denotes reflection. The fast-fast denotes fast P wave converted from fast P wave. The fast-slow denotes slow P wave converted from the fast P wave. The slow-fast denotes the fast P wave converted from the slow P wave. The slow-slow denotes the slow P wave converted from the slow P wave. The amplitudes and phases are the same as the potentials (Figure 7) and the errors (e and f) are small.

the solid and fluid phases, the amplitudes of the slow P waves in the solid phase are much smaller than that of the fast P waves; thus, it is more difficult to identify the slow P waves in the solid phase.

Figure 11 shows the separated P and S waves. The S waves are generated due to wave-mode conversion similar to the previous example. The separated fast and slow P waves are shown in Figure 12. The two
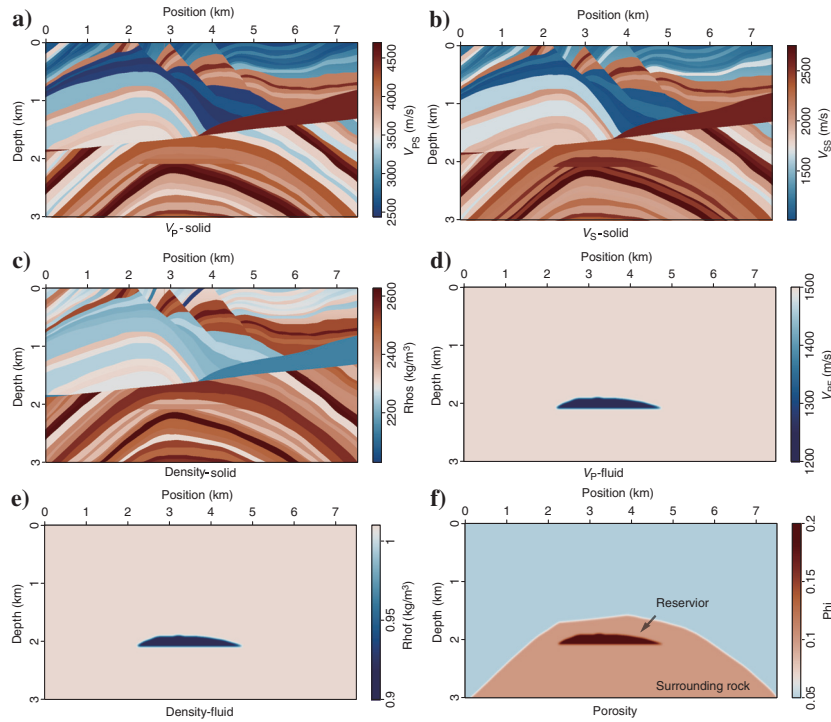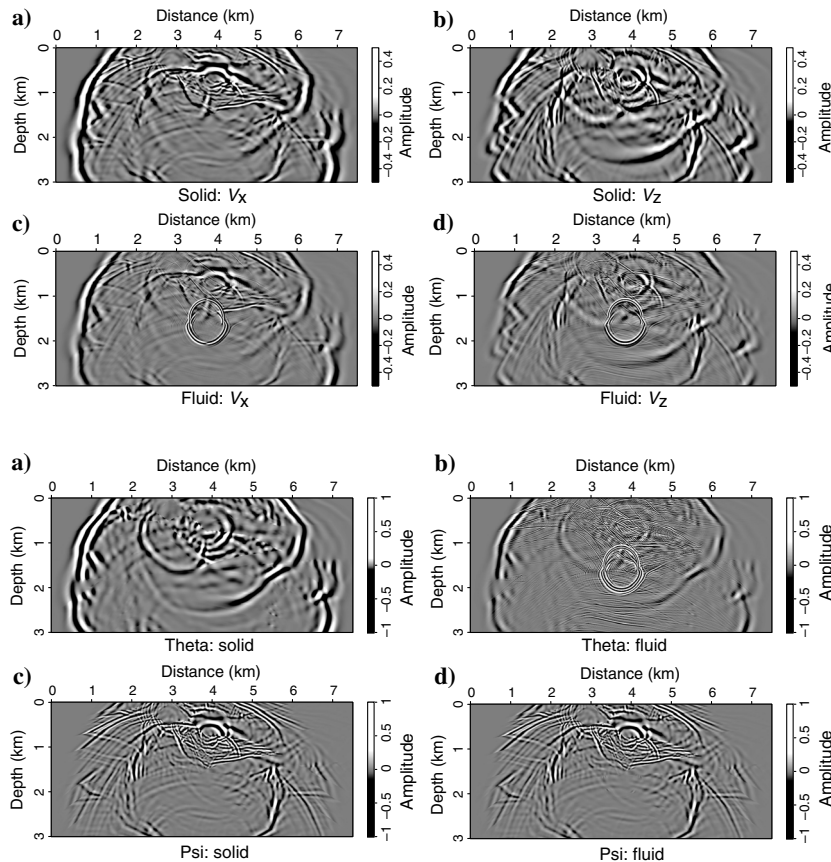


Figure 9. Parameters of the Marmousi2 model. (a) The $V_P$ model in the solid phase, (b) $V_S$ model in the solid phase, (c) $\rho_{solid}$ model, (d) $V_P$ model in the fluid phase, (e) $\rho_{fluid}$ model, and (f) the porosity model.



Figure 10. Components of the velocity wavefields in the Marmousi2 model. (a and b) Horizontal and vertical components of the solid phase, respectively. Because of the big difference between the velocity of the solid and fluid phase in this complicated model, the energy of the slow P waves in the solid phase is much smaller than that of the fast P waves; thus, it is very difficult to observe the slow P wave in the solid phase. The slow P waves in the fluid phase are clearer. It is the same for Figures 11 and 12. (c and d) Horizontal and vertical components of the fluid phase, respectively.



Figure 11. The P- and S-wave potentials based on Helmholtz decomposition in the Marmousi2 model. (a and b) The solid and fluid phases of P-wave potentials, respectively. (c and d) The S waves converted from the fast and slow P waves.

types of waves are separated clearly and keep the same amplitudes and phases as the input coupled P-wave potential. By summing the decomposed fast and slow P waves, we can reconstruct the wavefield

to compute the differences. The errors in Figure 12e and 12f illustrate that the proposed separation method has good accuracy even though the model has complicated structures.

Figure 12. Decomposed fast and slow P-waves components in the Marmousi2 model. (a and b) The fast and slow P waves in the solid phase, respectively. (c and d) The fast and slow P waves in the fluid phase, respectively. The separation results are good and the errors (e and f) are very small.
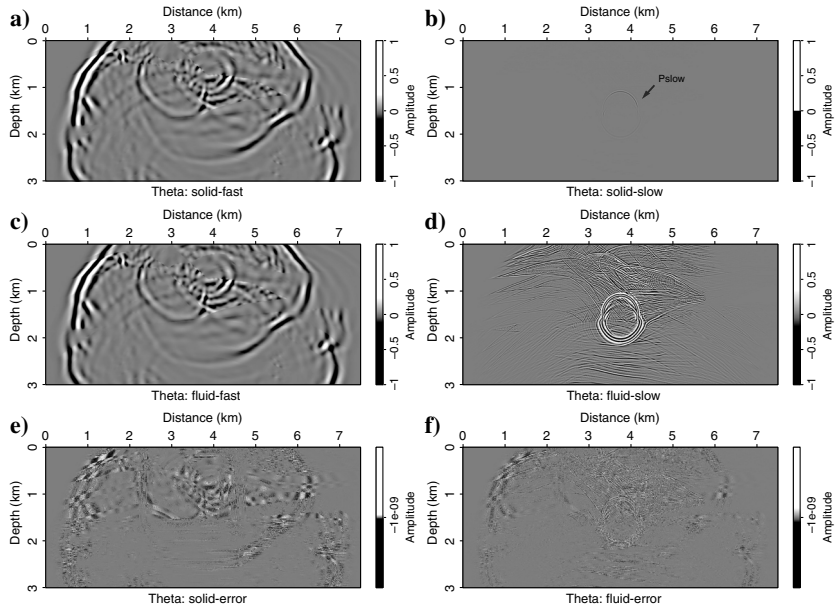


Figure 13. Results of decomposition when $B = 3000$. When $B$ is not zero, the fast and slow P waves can still be well separated using the proposed method. However, due to the effect of dissipation, the energy of the slow P waves decays rapidly whereas that of the fast P waves changes little.
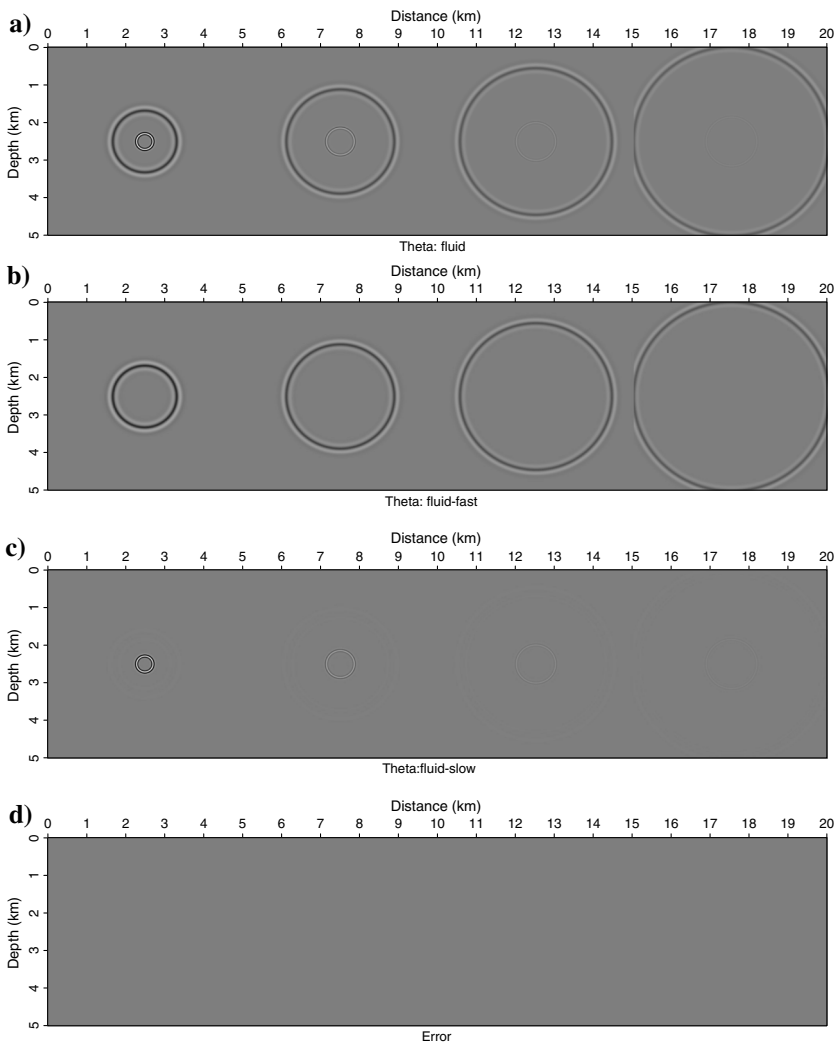
## DISCUSSION

To reduce the crosstalk artifacts in seismic imaging and inversion in the poroelastic medium, it is necessary to separate different wave modes accurately. Because the polarization directions of the fast and slow P waves are different from that of P and S waves, the methods used in the elastic medium can only separate P and S waves in the poroelastic medium but fail to extract the fast and slow P waves. By introducing a cross-product wave-mode separator, we provide a solution to decompose the poroelastic wavefields into S waves and fast and slow P waves in this study.

When using the proposed workflow, some aspects require careful consideration. First, in the derivations for eigenvalues and eigenvectors for P-wave potentials, we do not consider the energy dissipation in Biot's wave equations. Figure 13 presents an example of the wavefield separation with a dissipation parameter $B$ of 3000. Because the dissipation has a great influence on the slow P waves, the energy of slow P waves decays rapidly during propagation, whereas the fast P waves do not have a large change. However, the dissipation does not affect the wave propagation and polarization directions, the proposed method still produces accurate wavefield separation results, and their amplitudes are consistent with original wavefields. Second, the eigenvectors calculated in equation 10 are only determined by model parameters. They have the same form in the time-space and frequency-wavenumber domain; therefore, the numerical implementation does not involve hybrid-domain operation. The eigenvectors can be directly used as the separation operators.

In our study, the derivations and numerical examples are only for the 2D problem, but the hierarchical wavefield separation workflow can be directly extended to the 3D case. In a 3D problem, the displacements of solid and fluid phases have three components. After applying the Helmholtz decomposition, we can still obtain two potential wavefields ($\theta_s$ and $\theta_f$), which is the same as the 2D problem. Thus, the proposed decomposition strategy for the slow and fast P waves can be directly applied to the 3D problem. In addition, the proposed method also can be used to decompose different wave modes in an anisotropic medium. However, the propagation and polarization directions of each wave mode are neither parallel nor perpendicular and need to construct complicated cross-product separators, which require further investigation.

## CONCLUSION

In this study, we propose a method based on the eigenform analysis to completely separate the fast P wave, slow P wave, and S wave in the poroelastic medium. We first use the Helmholtz decomposition to compute the P- and S-mode potential wavefields to separate the two wave modes. Then, the eigenvalues and eigenvectors of the P-wave potentials for the solid and fluid phases are calculated. Using the eigenvectors, we can construct the separation operators to extract fast and slow P waves. The decomposed fast and slow P waves have the same amplitudes and phases as the coupled P-wave potentials. Numerical examples for a homogeneous model, a two-layer model, and the Marmousi2 model demonstrate the feasibility of the proposed wavefield separation method for a poroelastic medium.

## ACKNOWLEDGMENTS

## DATA AND MATERIALS AVAILABILITY

Data associated with this research are available and can be obtained by contacting the corresponding author.

## APPENDIX A

## DERIVATION OF THE CHRISTOFFEL EQUATION

The equations of P-wave potential wavefields (equation 3) are expressed as

$$\nabla^2[(A + 2N)\theta_s + Q\theta_f] = \frac{\partial^2}{\partial t^2}(\rho_{11}\theta_s + \rho_{12}\theta_f),$$

$$\nabla^2[Q\theta_s + R\theta_f] = \frac{\partial^2}{\partial t^2}(\rho_{12}\theta_s + \rho_{22}\theta_f). \quad \text{(A-1)}$$

We multiply the first equation with $\rho_{22}$ and the second equation with $\rho_{12}$ and obtain

$$\nabla^2[(A + 2N)\rho_{22}\theta_s + Q\rho_{22}\theta_f] = \frac{\partial^2}{\partial t^2}(\rho_{11}\rho_{22}\theta_s + \rho_{12}\rho_{22}\theta_f),$$

$$\nabla^2[Q\rho_{12}\theta_s + R\rho_{12}\theta_f] = \frac{\partial^2}{\partial t^2}(\rho_{12}^2\theta_s + \rho_{12}\rho_{22}\theta_f). \quad \text{(A-2)}$$

Then, we subtract the second equation from the first equation to eliminate $\theta_f$ on the right side and obtain

$$\nabla^2\{[(A + 2N)\rho_{22} - Q\rho_{12}]\theta_s + [Q\rho_{22} - R\rho_{12}]\theta_f\}$$
$$= \frac{\partial^2}{\partial t^2}(\rho_{11}\rho_{22} - \rho_{12}^2)\theta_s. \quad \text{(A-3)}$$

Similarly, we multiply the first equation with $\rho_{12}$ and the second equation with $\rho_{11}$ and obtain

$$\nabla^2[(A + 2N)\rho_{12}\theta_s + Q\rho_{12}\theta_f] = \frac{\partial^2}{\partial t^2}(\rho_{11}\rho_{12}\theta_s + \rho_{12}^2\theta_f),$$

$$\nabla^2[Q\rho_{11}\theta_s + R\rho_{11}\theta_f] = \frac{\partial^2}{\partial t^2}(\rho_{11}\rho_{12}\theta_s + \rho_{11}\rho_{22}\theta_f). \quad \text{(A-4)}$$

We subtract the second equation from the first equation to eliminate $\theta_s$ on the right side and obtain

$$\nabla^2\{[-(A + 2N)\rho_{12} + Q\rho_{11}]\theta_s + [-Q\rho_{12} + R\rho_{11}]\theta_f\}$$
$$= \frac{\partial^2}{\partial t^2}(\rho_{11}\rho_{22} - \rho_{12}^2)\theta_f. \quad \text{(A-5)}$$

We put equations A-3 and A-5 together and obtain (equation 4)

$$\nabla^2\{[(A+2N)\rho_{22}-Q\rho_{12}]\theta_s + [Q\rho_{22}-R\rho_{12}]\theta_f\}$$
$$= \frac{\partial^2}{\partial t^2}(\rho_{11}\rho_{22}-\rho_{12}^2)\theta_s,$$
$$\nabla^2\{[-(A+2N)\rho_{12}+Q\rho_{11}]\theta_s + [-Q\rho_{12}+R\rho_{11}]\theta_f\}$$
$$= \frac{\partial^2}{\partial t^2}(\rho_{11}\rho_{22}-\rho_{12}^2)\theta_f. \tag{A-6}$$

## APPENDIX B

## DERIVATION OF EIGENVALUE AND EIGENVECTORS

Assuming that the eigenvalue of the matrix $\mathbf{M}$ is $\lambda$, the corresponding eigenvector is $\eta$, and we have

$$\begin{bmatrix} (A+2N)\rho_{22}-Q\rho_{12} & Q\rho_{22}-R\rho_{12} \\ -(A+2N)\rho_{12}+Q\rho_{11} & -Q\rho_{12}+R\rho_{11} \end{bmatrix} \cdot \eta = \lambda \cdot \eta. \quad \text{(B-1)}$$

Then, we have

$$\begin{bmatrix} \lambda - ((A+2N)\rho_{22}-Q\rho_{12}) & R\rho_{12}-Q\rho_{22} \\ (A+2N)\rho_{12}-Q\rho_{11} & \lambda - (R\rho_{11}-Q\rho_{12}) \end{bmatrix} \cdot \eta = 0. \tag{B-2}$$

The eigenvalues $\lambda_1$ and $\lambda_2$ are determined by the following equation:

$$\lambda^2 - ((A+2N)\rho_{22}-2Q\rho_{12}+R\rho_{11})\lambda$$
$$+ [(A+2N)R-Q^2](\rho_{11}\rho_{22}-\rho_{12}^2) = 0. \tag{B-3}$$

Solving the equation, we can obtain the two solutions:

$$\lambda_{1,2} = \frac{(A+2N)\rho_{22}-2Q\rho_{12}+R\rho_{11}}{2} \pm \frac{\sqrt{C+D}}{2}, \quad \text{(B-4)}$$

where

$$C = (A+2N)^2\rho_{22}^2 + 2(A+2N)(2R\rho_{12}^2-R\rho_{11}\rho_{22}-2Q\rho_{12}\rho_{22}).$$
$$D = 4Q\rho_{11}(Q\rho_{22}-R\rho_{12}) + R^2\rho_{11}^2. \tag{B-5}$$

In addition, the corresponding eigenvectors are

$$\eta_1 = \begin{bmatrix} \frac{1}{2}[(A+2N)\rho_{22}-R\rho_{11}+\sqrt{C+D}] \\ -(A+2N)\rho_{12}+Q\rho_{11} \end{bmatrix}, \tag{B-6}$$

$$\eta_2 = \begin{bmatrix} Q\rho_{22}-R\rho_{12} \\ \frac{1}{2}[-(A+2N)\rho_{22}+R\rho_{11}-\sqrt{C+D}] \end{bmatrix}. \tag{B-7}$$

## APPENDIX C

## METHOD FOR DETERMINING $\mathbf{b}_{\text{fast}}$ AND $\mathbf{b}_{\text{slow}}$

Because the polarization vectors of fast and slow P waves are not perpendicular to each other, the angle between them is either acute or obtuse. We take how to determine $\mathbf{b}_{\text{fast}}$ as an example. In both cases, there are two vectors, $\mathbf{b}_{\text{fast\_1}}$ and $\mathbf{b}_{\text{fast\_2}}$, that are perpendicular
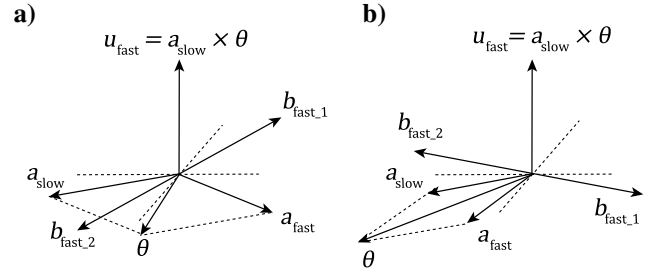


Figure C-1. Two possible cases of polarization directions of the fast and slow P waves. (a) The case where the polarization directions of the fast and slow P waves are at an acute angle and (b) the case at an obtuse angle. In both cases, $\mathbf{b}_{\text{fast\_1}}$ (the vector we need) and $\mathbf{a}_{\text{slow}}$ are at an obtuse angle. To obtain the coordinate of $\mathbf{b}_{\text{fast\_1}}$, we have to determine which of $(-y_1, x_1)$ and $(y_1, -x_1)$ satisfy equation C-2.

to $\mathbf{a}_{\text{fast}}$ and $\mathbf{u}_{\text{fast}}$, as can be seen in Figure C-1, where $\mathbf{a}_{\text{fast}}$ is the polarization vector of the fast P waves and $\mathbf{u}_{\text{fast}}$ is the separated fast wavefields. If we set $\mathbf{a}_{\text{fast}} = (x_1, y_1)$, the coordinate of $\mathbf{b}_{\text{fast\_1}}$ and $\mathbf{b}_{\text{fast\_2}}$ can be written as $(-y_1, x_1)$ or $(y_1, -x_1)$. (Each vector corresponds to one coordinate.) From Figure C-1, we can see that, in both cases, the angle $\alpha$ between the correct vector (we can remember it as $\mathbf{b}_{\text{fast\_1}}$) and $\mathbf{a}_{\text{slow}}$ is obtuse, where $\mathbf{a}_{\text{slow}}$ is the polarization vector of the slow P waves. If we set $\mathbf{a}_{\text{slow}} = (x_2, y_2)$, we have

$$\cos\alpha = \frac{\mathbf{b}_{\text{fast\_1}} \cdot \mathbf{a}_{\text{slow}}}{|\mathbf{b}_{\text{fast\_1}}||\mathbf{a}_{\text{slow}}|} = \frac{\mathbf{b}_{\text{fast\_1}} \cdot \mathbf{a}_{\text{slow}}}{\sqrt{x_1^2+y_1^2} \cdot \sqrt{x_2^2+y_2^2}} < 0, \quad \text{(C-1)}$$

and thus we have

$$\mathbf{b}_{\text{fast\_1}} \cdot \mathbf{a}_{\text{slow}} < 0. \tag{C-2}$$

Now that $\mathbf{a}_{\text{slow}} = (x_2, y_2)$, we only have to figure out which of $(y_1, -x_1)$ and $(-y_1, x_1)$ satisfy equation C-2. If $x_2y_1 - x_1y_2 < 0$, then $\mathbf{b}_{\text{fast}} = (y_1, -x_1)$. If $-x_2y_1 + x_1y_2 < 0$, then $\mathbf{b}_{\text{fast}} = (-y_1, x_1)$. Here, $\mathbf{b}_{\text{slow}}$ can be determined using a similar method.

## APPENDIX D

## DERIVATION OF $\mathbf{A}_{\text{fast}}$ AND $\mathbf{A}_{\text{slow}}$

We take $\mathbf{A}_{\text{slow}}$ as an example. If we set $\mathbf{a}_{\text{fast}} = (f_x, f_z)^T$, $\mathbf{a}_{\text{slow}} = (s_x, s_z)^T$, and $\mathbf{b}_{\text{slow}} = (b_x, b_z)^T$, $\theta = \theta_{\text{fast}} + \theta_{\text{slow}}$, where $\theta_{\text{fast}} = (\theta_{\text{solid}}^{\text{fast}}, \theta_{\text{fluid}}^{\text{fast}})^T$ and $\theta_{\text{slow}} = (\theta_{\text{solid}}^{\text{slow}}, \theta_{\text{fluid}}^{\text{slow}})^T$. We know that $\mathbf{a}_{\text{fast}}$ has the same direction as $\theta_{\text{fast}}$, and thus we have

$$\mathbf{a}_{\text{fast}} \times \theta_{\text{fast}} = 0. \tag{D-1}$$

Here, $\mathbf{a}_{\text{slow}}$ has the same direction as $\theta_{\text{slow}}$, and thus we have

$$\theta_{\text{slow}} = k\mathbf{a}_{\text{slow}}, \tag{D-2}$$

where $k$ is a constant. Then, we can make some derivation for $\mathbf{b}_{\text{slow}} \times (\mathbf{a}_{\text{fast}} \times \theta)$,

$$\mathbf{b}_{slow} \times (\mathbf{a}_{fast} \times \theta) = \mathbf{b}_{slow} \times (\mathbf{a}_{fast} \times (\theta_{fast} + \theta_{slow}))$$

$$= \mathbf{b}_{slow} \times (\mathbf{a}_{fast} \times \theta_{fast} + \mathbf{a}_{fast} \times \theta_{slow}) = \mathbf{b}_{slow} \times (\mathbf{a}_{fast} \times \theta_{slow})$$

$$= (\mathbf{b}_{slow} \cdot \theta_{slow})\mathbf{a}_{fast} - (\mathbf{b}_{slow} \cdot \mathbf{a}_{fast})\theta_{slow}$$

$$= (b_x \theta_{solid}^{slow} + b_z \theta_{fluid}^{slow})\begin{pmatrix} f_x \\ f_z \end{pmatrix} - (b_x f_x + b_z f_z)\begin{pmatrix} \theta_{solid}^{slow} \\ \theta_{fluid}^{slow} \end{pmatrix}$$

$$= \begin{pmatrix} (b_x \theta_{solid}^{slow} + b_z \theta_{fluid}^{slow})f_x \\ (b_x \theta_{solid}^{slow} + b_z \theta_{fluid}^{slow})f_z \end{pmatrix} - \begin{pmatrix} (b_x f_x + b_z f_z)\theta_{solid}^{slow} \\ (b_x f_x + b_z f_z)\theta_{fluid}^{slow} \end{pmatrix}$$

$$= \begin{pmatrix} b_z f_x \theta_{fluid}^{slow} - b_z f_z \theta_{solid}^{slow} \\ b_x f_z \theta_{solid}^{slow} - b_x f_x \theta_{fluid}^{slow} \end{pmatrix} = \begin{pmatrix} (f_x \theta_{fluid}^{slow} - f_z \theta_{solid}^{slow})b_z \\ (f_z \theta_{solid}^{slow} - f_x \theta_{fluid}^{slow})b_x \end{pmatrix}$$

$$= (f_x \theta_{fluid}^{slow} - f_z \theta_{solid}^{slow})\begin{pmatrix} b_z \\ -b_x \end{pmatrix} = (f_x s_z - f_z s_x)k\begin{pmatrix} b_z \\ -b_x \end{pmatrix}$$

$$= \begin{vmatrix} f_x & s_x \\ f_z & s_z \end{vmatrix} k\begin{pmatrix} b_z \\ -b_x \end{pmatrix}. \tag{D-3}$$

Now let us focus on $\mathbf{a}_{slow} = (s_x, s_z)^T$ and $\mathbf{b}_{slow} = (b_x, b_z)^T$. We know that $\mathbf{b}_{slow}$ is a vector that is perpendicular to $\mathbf{a}_{slow}$ and $\mathbf{a}_{fast} \times \theta$, and the coordinate of $\mathbf{b}_{slow}$ is represented by $\mathbf{a}_{slow}$ (see Appendix C), which means that $\mathbf{a}_{slow}$ and $\mathbf{b}_{slow}$ are perpendicular to each other and have the same magnitude.

Using the double cross-product operation $(\mathbf{b}_{slow} \times (\mathbf{a}_{fast} \times \theta))$, we have already repositioned the separated wavefields to the correct direction (the direction of $\mathbf{a}_{slow}$), which means that the vector $(b_z, -b_x)^T$ in equation D-3 has the same direction as $\mathbf{a}_{slow}$. In addition, $(b_z, -b_x)^T$ is perpendicular to $\mathbf{b}_{slow} = (b_x, b_z)^T$ and has the same magnitude as $\mathbf{b}_{slow}$. Thus, the vector $(b_z, -b_x)^T$ is $\mathbf{a}_{slow}$ and is equal to $(s_x, s_z)^T$. Equation D-3 becomes

$$\mathbf{b}_{slow} \times (\mathbf{a}_{fast} \times \theta) = \begin{vmatrix} f_x & s_x \\ f_z & s_z \end{vmatrix} k\begin{pmatrix} b_z \\ -b_x \end{pmatrix} = \begin{vmatrix} f_x & s_x \\ f_z & s_z \end{vmatrix} k\begin{pmatrix} s_x \\ s_z \end{pmatrix}$$

$$= \begin{vmatrix} f_x & s_x \\ f_z & s_z \end{vmatrix}\begin{pmatrix} \theta_{solid}^{slow} \\ \theta_{fluid}^{slow} \end{pmatrix}. \tag{D-4}$$

Thus, we have

$$\begin{pmatrix} \theta_{solid}^{slow} \\ \theta_{fluid}^{slow} \end{pmatrix} = \frac{1}{\begin{vmatrix} f_x & s_x \\ f_z & s_z \end{vmatrix}} \mathbf{b}_{slow} \times (\mathbf{a}_{fast} \times \theta). \tag{D-5}$$

Therefore, $\mathbf{A}_{slow} = [\mathbf{a}_{slow} \quad \mathbf{a}_{fast}]$. The $\mathbf{A}_{fast}$ can be verified using a similar process.

## APPENDIX E

### CONVERSION FORMULA FROM MODEL PARAMETERS TO BIOT PARAMETERS

The conversion formula is given by Geertsma and Smit (1961). We assume that the bulk modulus of air is zero. First, we calculate the bulk modulus of the solid and fluid:

$$K_s = \rho_{solid}\left(V_P^{solid^2} - \frac{4}{3}V_S^{solid^2}\right),$$

$$\mu_s = \rho_{solid}V_S^{solid^2},$$

$$K_f = \rho_{fluid}V_P^{fluid^2}, \tag{E-1}$$

where $K_s$ is the bulk modulus of the solid matrix, $\mu_s$ is the shear modulus of the solid matrix, and $K_f$ is the bulk modulus of the fluid. We assume that the pores are spherical and calculate the bulk modulus $K_d$ and shear modulus $\mu_d$ of the air-saturated medium:

$$\epsilon = \frac{\mu_s}{6}\frac{9K_s + 8\mu_s}{K_s + 2\mu_s},$$

$$K_d = \frac{4\mu_s K_s(1 - \phi)}{4\mu_s + 3\phi K_s},$$

$$\mu_d = \frac{\epsilon\mu_s(1 - \phi)}{\epsilon + \phi\mu_s}. \tag{E-2}$$

Then, we calculate the bulk modulus $K_k$ of the fluid-saturated medium using Gassmann's equation (Gassmann, 1951):

$$K_k = K_d + \frac{\left(1 - \frac{K_d}{K_s}\right)^2}{\frac{\phi}{K_f} + \left(1 - \frac{\phi}{K_s} - \frac{K_d}{K_s^2}\right)}. \tag{E-3}$$

Then, we have

$$L = \frac{1}{\frac{1 - \phi - \frac{K_k}{K_s}}{K_s} + \frac{\phi}{K_f}},$$

$$K = \left(1 - \frac{K_k}{K_s}\right)L,$$

$$H = \left(1 - \frac{K_k}{K_s}\right)^2 L + K_k + \frac{4}{3}\mu_d. \tag{E-4}$$

The elastic coefficients can be expressed as

$$A = H - 2K\phi + L\phi^2 - 2\mu_d,$$

$$N = \mu_d,$$

$$Q = K\phi - L\phi^2,$$

$$R = L\phi^2. \tag{E-5}$$

In addition, the mass coefficients are expressed as

$$\rho_{11} = (1 - \phi)\rho_{solid} + \frac{1}{2}(1 - \phi)\rho_{fluid},$$

$$\rho_{12} = \frac{1}{2}(\phi - 1)\rho_{fluid},$$

$$\rho_{22} = \frac{1}{2}(\phi + 1)\rho_{fluid}. \tag{E-6}$$

## REFERENCES

Aki, K., and P. G. Richards, 2002, Quantitative seismology: University Science Books.

Anthony, E., and N. Vedanti, 2022, An optimized staggered-grid finite-difference operator for seismic wave simulation in poroelastic media: Geophysics, **87**, no. 3, T225–T236, doi: 10.1190/geo2020-0240.1.

Biot, M. A., 1956a, Theory of propagation of elastic waves in a fluid-saturated porous solid. I. Low-frequency range: The Journal of the Acoustical Society of America, **28**, 168–178, doi: 10.1121/1.1908239.

Biot, M. A., 1956b, Theory of propagation of elastic waves in a fluid-saturated porous solid. II. Higher frequency range: The Journal of the Acoustical Society of America, **28**, 179–191, doi: 10.1121/1.1908241.

Biot, M. A., 1962, Mechanics of deformation and acoustic propagation in porous media: Journal of Applied Physics, **33**, 1482-1498, doi: 10.1063/1.1728759.

Carcione, J. M., H. B. Helle, and N. H. Pham, 2003, White's model for wave propagation in partially saturated rocks: Comparison with poroelastic numerical experiments: Geophysics, **68**, 1389–1398, doi: 10.1190/1.1598132.

Carcione, J. M., and S. Picotti, 2006, P-wave seismic attenuation by slow-wave diffusion: Effects of inhomogeneous rock properties: Geophysics, **71**, no. 3, O1–O8, doi: 10.1190/1.2194512.

Chen, K., 2011, First-order velocity-stress elastic wave field separation scheme for Biot two-phase isotropic medium: Chinese Journal of Computational Physics, **28**, 404.

Cheng, J., and S. Fomel, 2014, Fast algorithms for elastic-wave-mode separation and vector decomposition using low-rank approximation for anisotropic media: Geophysics, **79**, no. 4, C97–C110, doi: 10.1190/geo2014-0032.1.

de la Cruz, V., and T. Spanos, 1985, Seismic wave propagation in a porous medium: Geophysics, **50**, 1556–1565, doi: 10.1190/1.1441846.

Dellinger, J., and J. Etgen, 1990, Wave-field separation in two-dimensional anisotropic media: Geophysics, **55**, 914–919, doi: 10.1190/1.1442906.

Du, Q., C. Guo, Q. Zhao, X. Gong, C. Wang, and X. Li, 2017, Vector-based elastic reverse time migration based on scalar imaging condition: Geophysics, **82**, no. 2, S111–S127, doi: 10.1190/geo2016-0146.1.

Gassmann, F., 1951, Uber die elastizitat poroser medien: Vierteljahrsschrift der Naturforschenden Gesellschaft in Zurich, **96**, 1–23.

Geertsma, J., and D. Smit, 1961, Some aspects of elastic wave propagation in fluid-saturated porous solids: Geophysics, **26**, 169–181, doi: 10.1190/1.1438855.

Johnson, D. L., J. Koplik, and R. Dashen, 1987, Theory of dynamic permeability and tortuosity in fluid-saturated porous media: Journal of Fluid Mechanics, **176**, 379–402, doi: 10.1017/S0022112087000727.

Komatitsch, D., and R. Martin, 2007, An unsplit convolutional perfectly matched layer improved at grazing incidence for the seismic wave equation: Geophysics, **72**, no. 5, SM155–SM167, doi: 10.1190/1.2757586.

Mavko, G., and A. Nur, 1975, Melt squirt in the asthenosphere: Journal of Geophysical Research, **80**, 1444–1448, doi: 10.1029/JB080i011p01444.

Mavko, G. M., and A. Nur, 1979, Wave attenuation in partially saturated rocks: Geophysics, **44**, 161–178, doi: 10.1190/1.1440958.

Morse, P. M., and H. Feshbach, 1954, Methods of theoretical physics: American Journal of Physics, **22**, 410–413, doi: 10.1119/1.1933765.

Pride, S. R., J. G. Berryman, and J. M. Harris, 2004, Seismic attenuation due to wave-induced flow: Journal of Geophysical Research: Solid Earth, **109**, B01201, doi: 10.1029/2003JB002639.

Sahay, P. N., T. T. Spanos, and V. De La Cruz, 2001, Seismic wave propagation in inhomogeneous and anisotropic porous media: Geophysical Journal International, **145**, 209–222, doi: 10.1111/j.1365-246X.2001.00353.x.

Sripanich, Y., S. Fomel, J. Sun, and J. Cheng, 2017, Elastic wave-vector decomposition in heterogeneous anisotropic media: Geophysical Prospecting, **65**, 1231–1245, doi: 10.1111/1365-2478.12482.

Virieux, J., 1984, SH-wave propagation in heterogeneous media: Velocity-stress finite-difference method: Geophysics, **49**, 1933–1942, doi: 10.1190/1.1441605.

Virieux, J., 1986, P-SV wave propagation in heterogeneous media: Velocity-stress finite-difference method: Geophysics, **51**, 889–901, doi: 10.1190/1.1442147.

Wang, W., B. Hua, G. A. McMechan, and B. Duquet, 2018, P- and S-decomposition in anisotropic media with localized low-rank approximations: Geophysics, **83**, no. 1, C13–C26, doi: 10.1190/geo2017-0138.1.

Wang, W., and G. A. McMechan, 2015, Vector-based elastic reverse time migration: Geophysics, **80**, no. 6, S245–S258, doi: 10.1190/geo2014-0620.1.

White, J., 1975, Computed seismic speeds and attenuation in rocks with partial gas saturation: Geophysics, **40**, 224–232, doi: 10.1190/1.1440520.

White, J. E., N. Mihailova, and F. Lyakhovitsky, 1975, Low-frequency seismic waves in fluid-saturated layered rocks: The Journal of the Acoustical Society of America, **57**, S30–S30, doi: 10.1121/1.1995164.

Xiao, X., and W. S. Leaney, 2010, Local vertical seismic profiling (VSP) elastic reverse-time migration and migration resolution: Salt-flank imaging with transmitted P-to-S waves: Geophysics, **75**, no. 2, S35–S49, doi: 10.1190/1.3309460.

Yang, J., H. Zhang, Y. Zhao, and H. Zhu, 2019, Elastic wavefield separation in anisotropic media based on eigenform analysis and its application in reverse-time migration: Geophysical Journal International, **217**, 1290–1313, doi: 10.1093/gji/ggz085.

Yang, J., H. Zhu, W. Wang, Y. Zhao, and H. Zhang, 2018, Isotropic elastic reverse time migration using the phase-and amplitude-corrected vector P- and S-wavefields: Geophysics, **83**, no. 6, S489–S503, doi: 10.1190/geo2018-0023.1.

Yang, Q., and A. Malcolm, 2021, Frequency domain full-waveform inversion in a fluid-saturated poroelastic medium: Geophysical Journal International, **225**, 68–84, doi: 10.1093/gji/ggaa579.

Zhang, Q., and G. A. McMechan, 2010, 2D and 3D elastic wavefield vector decomposition in the wavenumber domain for VTI media: Geophysics, **75**, no. 3, D13–D26, doi: 10.1190/1.3431045.

Zhu, H., 2017, Elastic wavefield separation based on the Helmholtz decomposition: Geophysics, **82**, no. 2, S173–S183, doi: 10.1190/geo2016-0419.1.

Zhu, X., and G. McMechan, 1991, Numerical simulation of seismic responses of poro-elastic reservoirs using Biot theory: Geophysics, **56**, 328–339, doi: 10.1190/1.1443047.

Biographies and photographs of the authors are not available.